JOURNAL OF MATERIALS SCIENCE **36** (2001) 189–199

Tribological behavior and wear mechanisms of Ti-C : H/TiC/TiCN/TiN/Ti coatings when sliding against steel, bronze and aluminum alloy rods

Y. L. SU
Department of Mechanical Engineering, National Cheng Kung University, Tainan, Taiwan
E-mail: suyl@mail.ncku.edu.tw

W. H. KAO
Department of Fundamental Science, China Air Force Aeronautical and Technical School, Gangshan

$Ti_{x\%}$-C : H coatings of differing thicknesses and with various titanium concentrations were deposited on tungsten carbide disks by unbalanced magnetron sputtering. The mechanical properties, microstructure, and adhesion strength of these coating were measured. The tribology properties of the coatings against AISI 1045 steel, AA7075, AA6061 aluminum alloy, and bronze rods were tested by an oscillation sliding test machine with a line-contact wear mode under dry conditions. The microhardness of $Ti_{x\%}$-C : H coatings increased with an increasing Ti concentration. The optimum coatings are composed of an intermediate layer of TiC/TiCN/TiN/Ti and a top layer of $Ti_{x\%}$-C : H with $x \leq 20\%$. These coatings have an excellent wear resistance and a low friction coefficient when paired with a carbon steel or copper alloy. These pairs are marked by the mildly wear of the counterbodies of AISI 1045 steel and bronze. The coatings are less suitable for oscillation with the aluminum alloy under dry conditions due to severe adhesion damage.

1. Introduction

According to precursory investigations, diamond like carbon (DLC) or amorphous hydrogenated carbon (a-C : H) possesses an extreme hardness (2000–10000 HV) depending on the deposition methods and conditions [1, 2]. These carbon films also have extremely low friction and high wear resistance on sliding interface [3–7]. They have been successfully used as a low load protective for magnetic and optical disks because of these characteristics [8, 9]. The DLC coating adhesion has been improved by both a graded transition from TiN-TiCN layer to amorphous hydrogenated carbon layer [10] and a multiple stack of metal/DLC and carbide/DLC nanolayers [11]. A recent investigation presented a functionally gradient design using a gradual metal/ceramic/DLC transition in which load support and adhesion strength were improved [12–14]. Furthermore, some studies have advocated metal doping of the DLC layer to reduce the internal stress of DLC coating [15–17].

A potential coating for a film should be multicomponent and multilayer because they perform better than single layer coatings and they also contain attractive properties of different materials as shown in various single protective layers.

This study investigates the wear and friction behavior of the graded intermediate layer of TiC/TiCN/TiN/Ti combined with various Ti concentration of Ti-C : H coatings in contact with AISI 1045 steel, AA7075 aluminum alloy, AA 6061 aluminum alloy and with bronze rods by a reciprocating test machine. The optimum coating films are determined as a function of Ti concentration, coating thickness, and coating composition.

2. Experiment

2.1. Specimens preparation

The materials used for the upper specimens in the SRV (Schwingung Reibungund Verschleiss) oscillation friction and wear tester were AISI 1045 steel (Hv 286, 50 g), AA 6061-T651 (Hv 136, 50 g), AA7075-T651 (Hv 258, 50 g) aluminum alloy, and bronze (Hv 261, 50 g) rods. The substrate material of the lower specimen was a tungsten carbide (WC) bulk disk (Hv 1740, 50 g). The rod specimens were machined and cut off directly from round AISI 1045 steel, AA 6061-T651, AA7075-T651 aluminum alloy, and bronze rods. Their surfaces were then mechanically polished to a roughness of $Ra \approx 0.32\ \mu m$. The WC bulk disk was a powder metallurgy sintered part containing 6 wt% Co. The average size of WC particle was around $0.5\ \mu m$. The fully mixed powder of WC and Co were compressed to a density of 14.73 gcm^{-3}, followed by a pre-sinter at 600–1000°C for 30 min., and then sintered in a vacuum for 2–3 hour at 1450–1500°C [18]. All the specimens were fabricated to a shape suitable for the SRV holder. After all, these specimens were ultrasonically cleaned

in acetone, and were kept in an electric-dryer to prevent the surface from pollution again.

2.2. Coatings deposition

Coatings were deposited on tungsten carbide (WC) bulk disks based on a technique using an unbalanced magnetron (UBM) sputtering (UDP- 450, Teer Coatings, UK) process and a closed-loop optical emission monitoring (OEM) control system. Sputtering was performed in an Ar atmosphere and N_2 and C_2H_2 were used as reaction gases. For instance, the process of coating Ti-C : H/TiC/TiCN/TiN/Ti/substrate deposition is as following:

First a layer of Ti of about 0.1 μm thick is deposited on each of the specimens. After deposition of the Ti layer, nitrogen is introduced to produce a layer of TiN. Then, C_2H_2 is introduced gradually to produce a TiCN layer. After then, gradually turn off provision of the nitrogen and increase the flow of C_2H_2 at the same time to produce a TiC layer. Finally, the C_2H_2 flow is further increased gradually to cause more poisoning of the Ti target. An optical emission spectrometer is used to measure the intensity of Ti emission from one of the targets. The C_2H_2 flow is then admitted through a piezoelectric valve until the intensity of the emission line has dropped to a pre-selected value. The spectrometer and the piezoelectric valve are then switched into a closed -loop system to stabilize partial pressure of the reactive gas at this level. As a result, the Ti metal and hydrocarbon is sputtered simultaneously from the poisoned target surface to produce a $Ti_{x\%}$-C : H layer. OEM control allows the deposition of films with the required metal composition formed by monitoring the ratio, x%, of target "poisoning" in the relative intensity of the selected titanium emission line reference to the intensity from a non-poised target. The final composition of the $Ti_{x\%}$-C : H coating will depend on the degree of this target poisoning by the hydrocarbon. Table I displays the parameters of deposition. The coating films consist of $Ti_{x\%}$-C : H with $x = 10\%$, 20%, and 30% target "poisoning" levels with various film thickness. A intermediate layer TiC/TiCN/TiN/Ti with 2.6 μm thickness was deposited on the WC substrate under the $Ti_{x\%}$-C : H topcoats (cases 1–9). In addition, a gradual $Ti_{10\%}$-C : H/$Ti_{20\%}$-C : H/$Ti_{30\%}$-C : H/Ti/substrate (case 10), an intermediate layer TiC/TiCN/TiN/Ti/substrate (case 12), and a gradual topcoat of $Ti_{10\%}$-C : H/$Ti_{20\%}$-C : H/$Ti_{30\%}$-C : H with intermediate layer TiC/TiCN/TiN/Ti (case 11) were deposited on the WC substrate as shown in Table II.

TABLE I The depositions parameters for the $Ti_{x\%}$-C : H coatings

Parameters	$Ti_{x\%}$-C : H coatings
Reaction gases	N_2 & C_2H_2
Chamber pressure (Pa)	1
Bias voltage (V)	−50
Target current (A)	6
Chamber temperature (°C)	150
Deposition rate (μm/hr)	2

2.3. Test apparatus

The microhardness and elastic deformation energy of the coating films were measured by a nanoindentation tester (Fischer Fischeroscopy H100B, Germany). Herein, the force at initial contact was 0.4 mN, time between two load steps was 1 sec., total time for loading was 39 sec., and the force at final contact was 100 mN. In this work, for each case, 5 to 10 indents were performed.

A diamond stylus of diameter 300 μm was driven across the coatings to determine the coating-to-substrate adhesion at a continuously increased loading rate of 1 N s^{-1}. The nominal maximum load was 70 N. Each case was subjected to five scratch tests to determine critical loads for coating adhesion valuation.

Wear tests were also performed using a SRV tester (Optimol, Germany). The configuration of the SRV test machine consisted of a fixed lower specimen supporter and a replaceable upper specimen holder. The upper specimen was a rod, while the lower specimen was a

TABLE II Film thickness, hardness, elastic recovery energy, and elements composition of various coatings

Case No.	Ti target poisoning (%)	Ti-C : H thickness (μm)	TiC/TiCN/ TiN/Ti thickness (μm)	Hardness (Kg/mm^2)	Elastic deformation energy (%)	Elements composition (at %)			
						Ti	C	N	O
1	10	1.5	2.5	1390	75.2	3.5	90.2	2.8	3.5
2	10	2.5	2.5	931	78.4	3.5	90.2	2.8	3.5
3	10	3.5	2.5	801	81.3	3.5	90.2	2.8	3.5
4	20	1.5	2.5	1579	72.0	7.7	82.6	3.2	6.5
5	20	2.5	2.5	1399	72.2	7.7	82.6	3.2	6.5
6	20	3.5	2.5	1244	77.0	7.7	82.6	3.2	6.5
7	30	1.5	2.5	2946	58.9	34.4	58.9	4.1	2.6
8	30	2.5	2.5	2743	53.4	34.4	58.9	4.1	2.6
9	30	3.5	2.5	2486	55.7	34.4	58.9	4.1	2.6
10	graded 30 → 20 → 10	5.0	0	980	78.7	3.5	90.2	2.8	3.5
11	graded 30 → 20 → 10	2.5	2.5	1468	78.5	3.5	90.2	2.8	3.5
12	-----	0	5.0	2983	54.8	-----	-----	-----	-----
wc	-----	-----	-----	1740		-----	-----	-----	-----

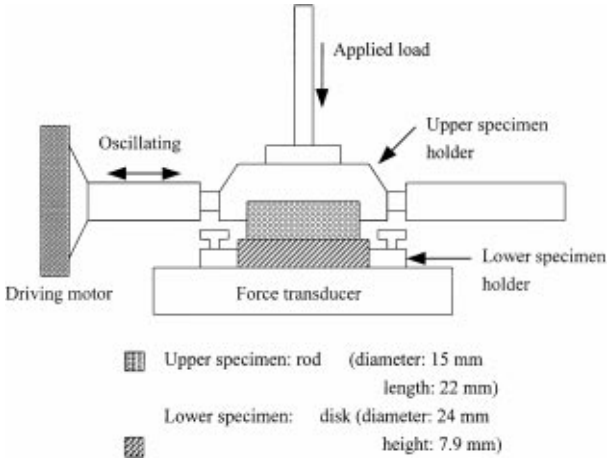

Figure 1 SRV wear test machine.

disk in this test. Fig. 1 displays the dimensions of the test specimens and a schematic diagram of the experiment set up.

The arrangement of a rod mated with a disk formed a rod-on-disk line contact wear mode. The tests were performed at room temperature, atmospheric pressure, and under unlubricated conditions. The relative humidity of the laboratory was about 45–55%. In addition, a constant 1mm stroke, 100 N normal load, a 24-min. test duration (144 m sliding distance), and a 50 Hz frequency were employed. The maximum depth of the wear scars on the lower test contacted disk was measured by a surface profilometer (Kosake SE30H, Japan) with a precision of $\pm 0.005\,\mu$m at a magnification of $\times 10^6$. All tests were performed twice, and three different measurements were taken from each pass of the tests. Then, each of the six measurements from the same test was averaged and shown as the measured results in this work.

2.4. Observation equipment

The worn surface, fracture mechanism, constitution and metallographic structure of the coating layer were observed by a scanning electron microscope (SEM), X-ray mapping (wavelength dispersive spectrometer (WDS) and energy dispersive spectrometer (EDS)) and Raman instrument, respectively.

3. Results

3.1. Raman spectra

The Raman spectra of $Ti_{x\%}$-C : H film has two broad peaks near 1385 cm^{-1} and 1579 cm^{-1}. It is reported

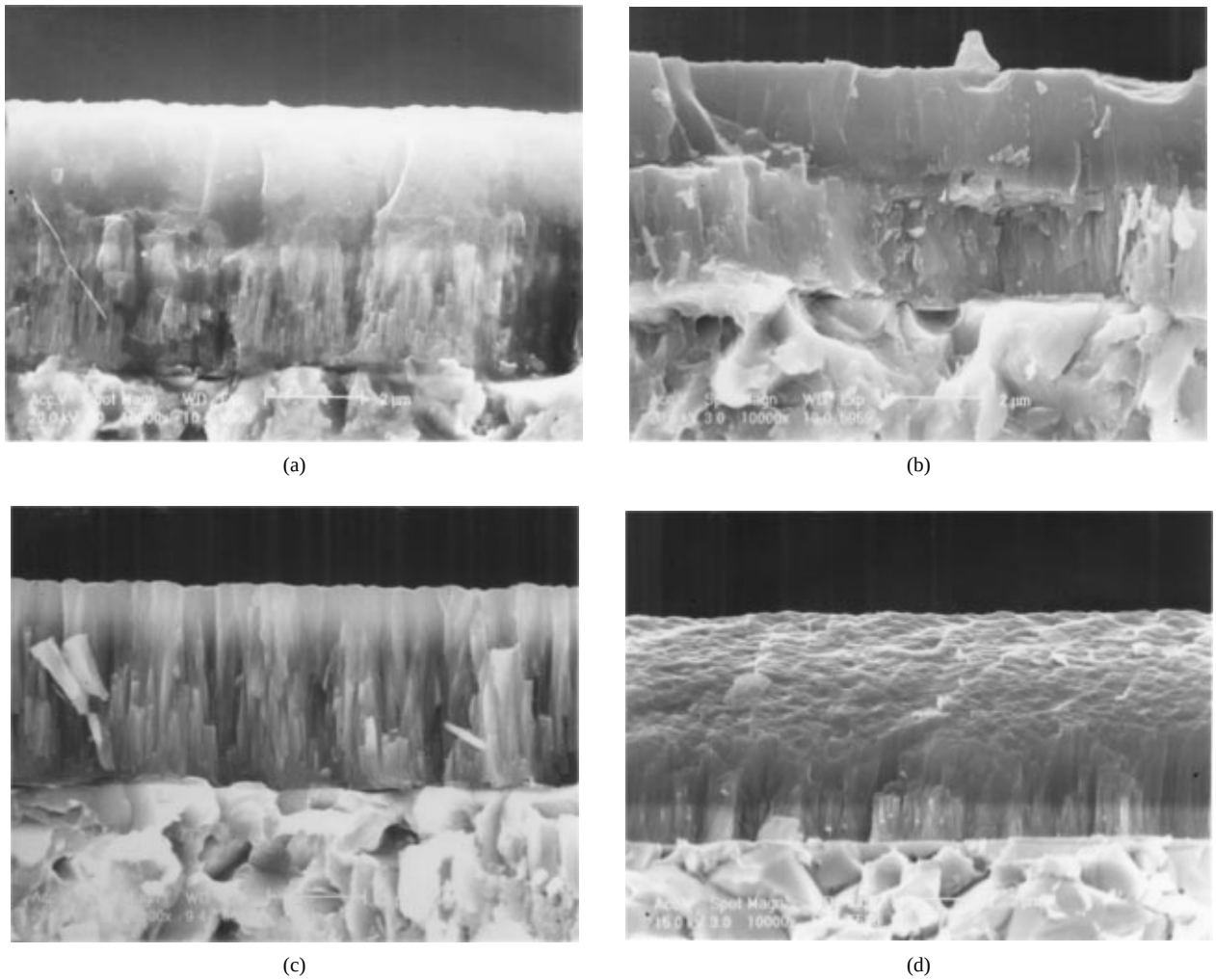

Figure 2 The typical cross section fractures of $Ti_{x\%}$-C : H/TiC/TiCN/TiN/Ti coatings with diffrent x% level, (a) $x = 10\%$, (b) $x = 20\%$, (c) $x = 30\%$, and of (d) graded $Ti_{x\%}$-C : H coating from $x = 30\%$ to $x = 10\%$ (from substrate to top surface), respectively.

that graphite-like carbon shows Raman peaks near 1360 cm^{-1} and 1600 cm^{-1}, whereas no significant peak is found near 1550 cm^{-1} which is said to appear in amorphous-like carbon [19, 20]. Therefor, based on these results, the $Ti_{x\%}$-C : H films are estimated to be mainly composed of amorphous-like carbon.

3.2. Coating microstructure

Fig. 2a–d depict the typical scanning electron photomicrographs of fracture sections of $Ti_{x\%}$-C : H coatings, produced at different levels of Ti target "poisoning". In these figures, microstructure of $Ti_{x\%}$-C : H coatings changed when varying the x% values. Fig. 2a and b illustrate the typical microstructures of coatings with $x = 10\%$ and $x = 20\%$ of poisoning level, representing two parts, respectively. One part is an intermediate layer (TiC/TiCN/TiN/Ti) possessing a well-developed columnar structure with free growth of columns from the substrate. Meanwhile, the other part, $Ti_{x\%}$-C : H coating appears quite dense in which the amorphous structure expands from intermediate layer to the coating surface. If the coating has $x = 30\%$ level, the microstructure of $Ti_{30\%}$-C : H coating changed into a columnar structure, expanding from the intermediate layer to the coating surface (Fig. 2c). Fig. 2d displayed the graded $Ti_{x\%}$-C : H films which poisoning level gradually from 30% to 10%. Table II lists the composition of the $Ti_{x\%}$-C : H coatings with varying ratios of target "poisoning" as analyzed by WDS. The $x = 10\%$ and $x = 20\%$ poisoning levels indicate that the coatings contain approximately 90% and 82% of carbon atomic, respectively. However, at $x = 30\%$ poisoning level, the percentage of carbon atomic markedly decreases to 59% while the percentage of titanium atomic significantly increases to 34%. Obviously, the $Ti_{x\%}$-C : H coatings with different x% level values may lead to a difference in film mechanical properties, and tribological behavior. The following sections more closely examine these phenomena.

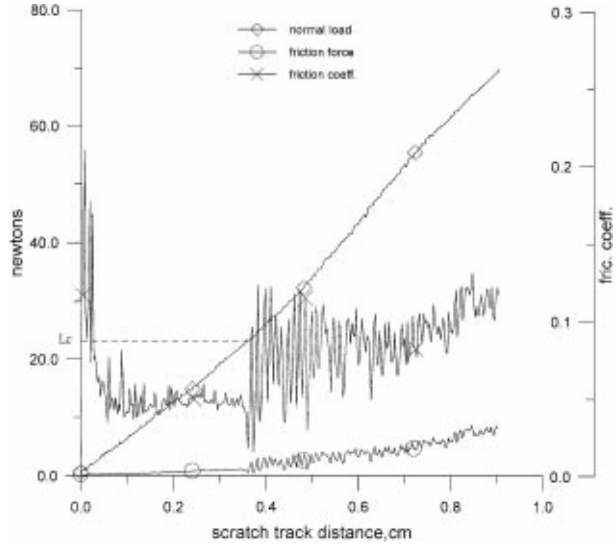

Figure 3 Typical scratch testing showed normal load, frictional force, and friction coefficient vs. scratch track distance of $Ti_{30\%\text{-}20\%\text{-}10\%}$-C : H coating (case 10).

3.3. Hardness and adhesion strength

Table II reveals that the microhardness and the elastic deformation energy of the coating films are in opposition to each other. That is, the microhardness increases and the elastic deformation decreases with an increase in the Ti-metal concentration (increasing x% level). Indeed, the microhardness of the films significantly increases when the $Ti_{x\%}$-C : H coatings are at $x = 30\%$ level. Such an increase is attributed to the structural alteration (described in Section 3.1) and the formation of larger amounts of hard titanium carbide clusters in the soft $Ti_{x\%}$-C : H matrix [21].

The adhesion strength strongly correlates with the coating composition and Ti concentration according to the scratch test results (see Table III). The friction coefficients were recorded continuously during the tests. The scratch results indicate that there are three types of adhesion strength at different coating films.

TABLE III The friction coefficient (F_C) before the coating spallation, friction coefficient (F_f) after coating spallation failure, and critical load (Lc) of scratch test. The wear depth (D) and the friction coefficient (F) of the coating disks sliding against the 1045 steel (D_S, F_S), the bronze (D_b, F_b), the aluminum alloy 7075 (D_{a7}, F_{a7}), and the aluminum alloy 6061 (D_{a6}, F_{a6}) of SRV test. Wear on disk is measured in depth

Case No.	Scratch test			SRV test							
	Friction coefficient		Critical load (N)	Wear depth (μm)				Friction coefficient			
	F_C	F_f	Lc	D_S	D_b	D_{a7}	D_{a6}	F_S	F_b	F_{a7}	F_{a6}
1	0.07	----	>70	1.9	1.8	4.2	2.6	0.32	0.35	0.51	0.67
2	0.07	----	>70	1.5	1.5	5.1	3.0	0.34	0.31	0.49	0.66
3	0.06	----	>70	2.5	2.4	5.0	6.0	0.35	0.33	0.47	0.59
4	0.06	----	>70	2.2	2.2	4.1	3.0	0.30	0.32	0.50	0.63
5	0.07	----	>70	2.2	2.3	4.5	4.0	0.28	0.33	0.51	0.60
6	0.06	----	>70	2.9	2.7	4.9	6.0	0.28	0.29	0.53	0.58
7	0.21	0.22	62	5.3	2.7	3.3	3.5	1.44	0.70	0.53	0.67
8	0.18	0.21	61	5.4	3.0	4.0	4.8	1.26	0.67	0.58	0.71
9	0.19	0.27	56	6.1	3.6	4.5	6.1	1.06	0.64	0.59	0.71
10	0.06	0.09	23	1.8	2.6	5.5	5.5	0.27	0.30	0.50	0.64
11	0.06	----	>70	2.8	1.9	6.0	6.1	0.32	0.32	0.48	0.64
12	0.17	0.24	21	4.1	3.4	6.0	5.8	0.71	0.65	0.52	0.70
WC				3.2	2.7	0.0	0.0	0.95	1.04	0.72	0.61

The first type of typical failure pertained to the TiC/TiCN/TiN/Ti (case 12) and the $Ti_{30\%\text{-}20\%\text{-}10\%}$–C : H coatings (case 10). The coatings exhibited a high mean value of 0.17 (case 12) friction coefficients and a low mean value of 0.06 (case 10) friction coefficients before the coatings' spallation. Both their mean values of friction coefficients increased (see Table III) after the coatings spallation. Fig. 3 illustrates the typical curves (case 10) of the normal load, frictional force, and friction coefficient vs. scratch track distance. The friction coefficient and fluctuation increased as the coating spalled. The critical load (Lc) of the coating films is defined as the load applied when the substrate started to be revealed in the scratch track. Case 10 and case 12 have relatively low critical loads of Lc = 23 N and Lc = 21 N as listed in Table III. Deposited coatings generate a large internal stress at lower temperatures, which increases as the coating thickness expands, yielding a poor adhesion to the coatings. The second type of typical failure occurred when the $Ti_{30\%}$-C : H coatings combined with the intermediate TiC/TiCN/TiN/Ti coating (cases 7–9). These coatings displayed high mean friction coefficients of 0.18–0.21 (see Table III) but the adhesion strength improved corresponding to the high critical load 62 N, 61 N, and 56 N of each case. The $Ti_{x\%}$–C : H/TiC/TiCN/TiN/Ti coatings with $x = 10\%$ and $x = 20\%$ levels (cases 1–6 and 11) did not reveal any crack, flaking, or tearing on scratch channel and ridges of the coatings. All the measured scratch depth of the coatings were about 1.4 μm–1.6 μm and all had low mean friction coefficients that were about 0.06–0.07 (see Table III) throughout the scratch tests. This phenomenon is attributed to (1) the multilayer design of the $Ti_{x\%}$-C : H/TiC/TiCN/TiN/Ti coatings which decreased the internal stress; (2) the better energy absorption of the top coating $Ti_{x\%}$-C : H due to greater elastic deformation and low friction force between the contact surface. Hence, crack, flaking, or tearing of the coatings is avoided.

The coating $Ti_{x\%}$–C : H without an intermediate layer (case10) and the coating TiC/TiCN/TiN/Ti without top layer of $Ti_{x\%}$-C : H (case 12) display the worst adhesion strength. The coatings (cases 7–9) with high Ti-concentration also have higher friction coefficients that caused lower adhesion strength. The optimum coating composition is an intermediate layer and top layer of $Ti_{x\%}$-C : H with $x = 10\%$ and $x = 20\%$ levels.

3.4. Characterization of wear and friction

3.4.1. Coatings against 1045 steel and bronze

Friction coefficients were also continuously recorded during the SRV tests and the wear results and mean values of friction coefficients are classified in Table III. The $Ti_{x\%}$-C : H coatings with $x = 10\%$ and $x = 20\%$ levels (cases 1–6) and $Ti_{30\%\text{-}20\%\text{-}10\%}$-C : H (cases 10 and 11) have a lower wear depth on the coating and low friction coefficients of about 0.27–0.35 against a 1045 steel rod and about 0.29–0.35 against a bronze rod. Case 10 shows that good wear resistance does not correspond to poor adhesion strength, but can be attributed to a line–contact mode with a low normal load and a low friction coefficient that forms a lower shear stress between the contact surfaces. Therefore, the shear stress cannot induce coating failure during the wear test. On the other hand, the maximum wear depth and high friction coefficients of 0.71–1.44 against 1045 steel and of 0.64–0.69 against bronze for the $Ti_{x\%}$-C : H coatings with $x = 30\%$ level (cases 7–9) and TiC/TiCN/TiN/Ti coating (case 12) against 1045 steel rods and bronze rods.

The coatings with $Ti_{x\%}$-C : H with $x = 10\%$ and $x = 20\%$ have good wear resistance and low friction coefficient in contact with 1045 steel and bronze rods as compared with the WC substrate. Conversely, the $Ti_{30\%}$-C : H coatings (cases 7–9) and the TiC/TiCN/TiN/Ti coating (case 12) have poor wear resistance and high friction coefficients even though these coatings are harder than the others.

Table III demonstrates that the coating thickness influences the wear resistance as all of the $Ti_{x\%}$-C : H coatings with 1.5 μm thickness were worn out after their tests. In addition, all of the the $Ti_{x\%}$-C : H coatings with 3.5 μm thickness have a deeper wear depth on the coated disks. However, the films with 2.5 μm thickness and $x = 10\%$ level (case 2) exhibit the optimum wear resistance.

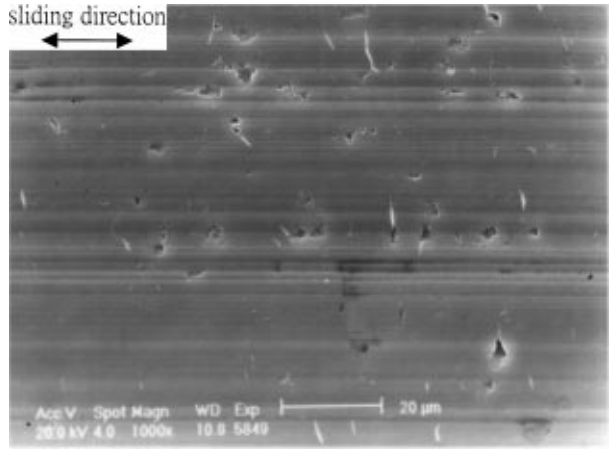

(a)

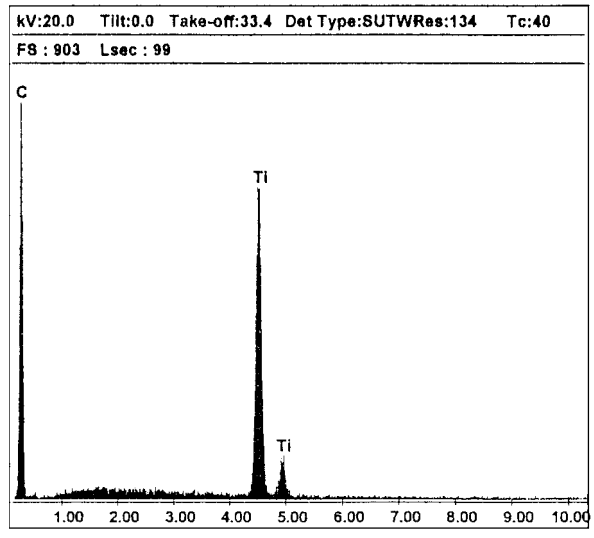

(b)

Figure 4 (a) Typical wear surface of $Ti_{x\%}$-C : H coating with $x = 10\%$ or $x = 20\%$, sliding against AISI 1045 steel rod, (b) corresponding EDS analysis of (a).

3.4.2. Coatings in contact with 7075 Al and 6061 Al

The 7075Al/coating and 6061Al/coating sliding wear pairs displayed similar wear mechanisms independent of their hardness. All of the coatings have high friction coefficients (Table III) with large fluctuation (a range about 0.4–0.8 for each wear pair) against 7075 Al and 6061 Al rods. Furthermore, all the coatings have severe wear (Table III) sliding against the 7075 and the 6061 aluminum alloy. The severe wear and the high friction coefficient because the adhesion behavior took place on the contact surfaces between the coating film and the Al rod under dry conditions. It may be due to the aluminum alloy with low melting point, easily softened in contact surface and adhered to coated disk which formed a large and lapped transfer layer that induced severe wear between the $Ti_{x\%}$-C : H and the 7075Al or 6061 Al contact surfaces. Conversely, the WC substrate has excellent wear resistance against aluminum alloy (zero wear on WC substrate).

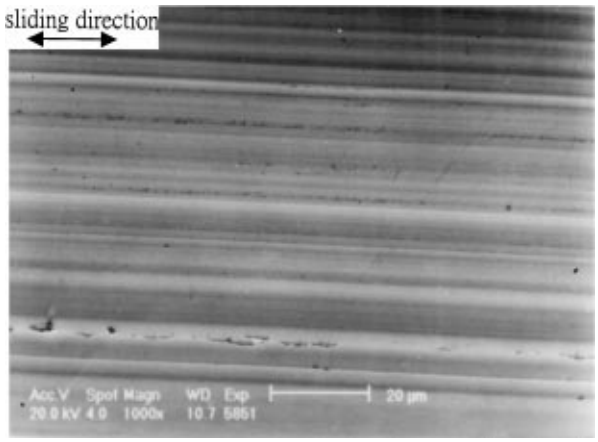

Figure 5 Typical wear surface of $Ti_{x\%}$-C : H coating with $x = 10\%$ or $x = 20\%$, sliding against bronze rod.

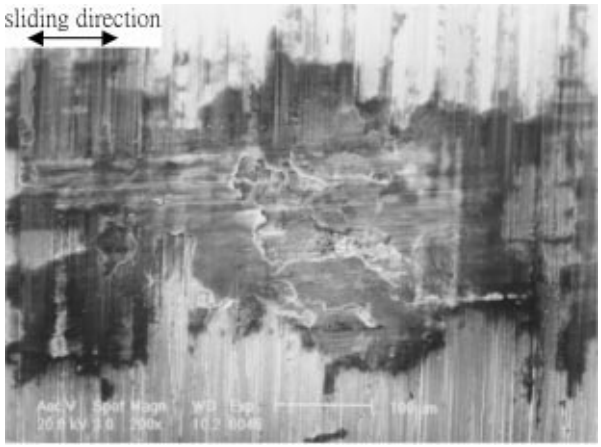

(a)

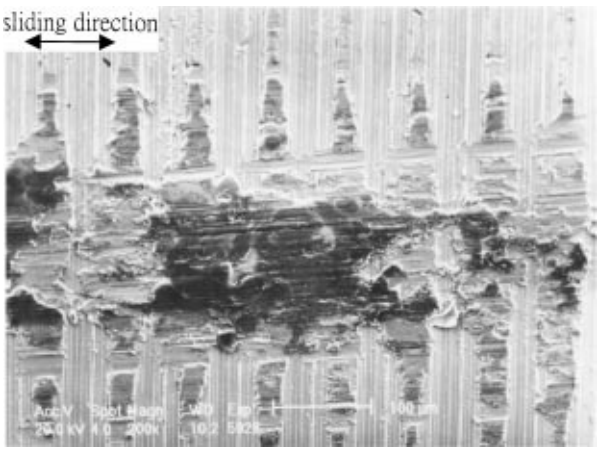

(b)

Figure 6 Typical SEM photomicrograph of wear scar on (a) AISI 1045 steel rod, (b) bronze rod, sliding against $Ti_{x\%}$-C : H coating with $x = 10$ or $x = 20$ level.

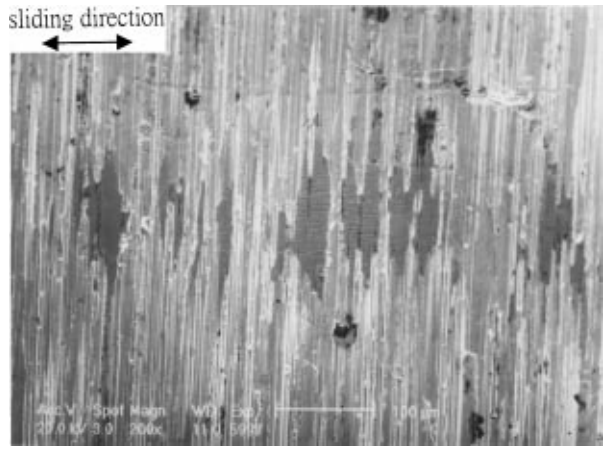

(a)

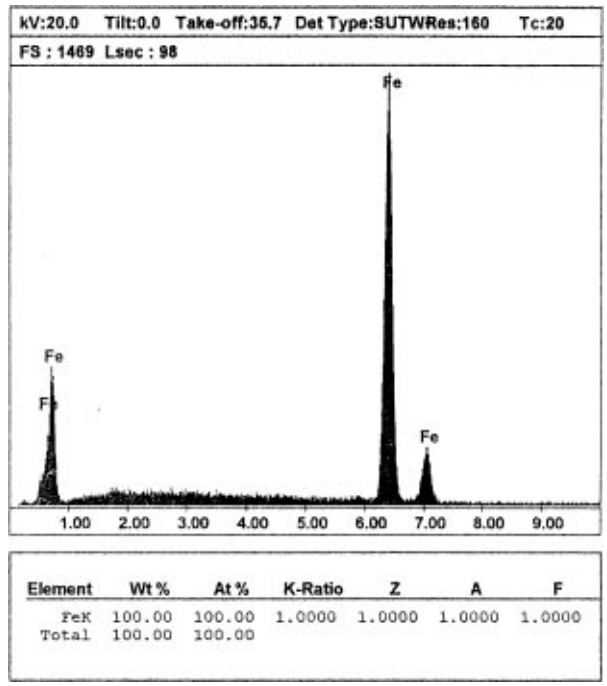

(b)

Figure 7 (a) Typical SEM photomicrograph of wear scar on AISI 1045 steel rod, and (b) EDS analysis of (a), sliding against $Ti_{10\%}$-C : H or $Ti_{20\%}$-C : H coatings after wear testing for 30 seconds.

4. Wear mechanism

4.1. $Ti_{x\%}$-C : H/1045 steel and $Ti_{x\%}$-C : H/ bronze wear pairs

The tribological behavior of coatings can be classified into two groups.

Group 1: $Ti_{x\%}$-C : H coatings with $x = 10\%$ and $x = 20\%$ levels (cases 1–6, 10, and 11) in which the

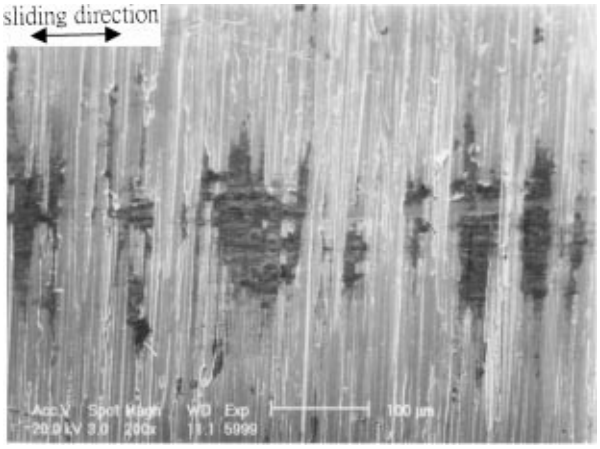

(a)

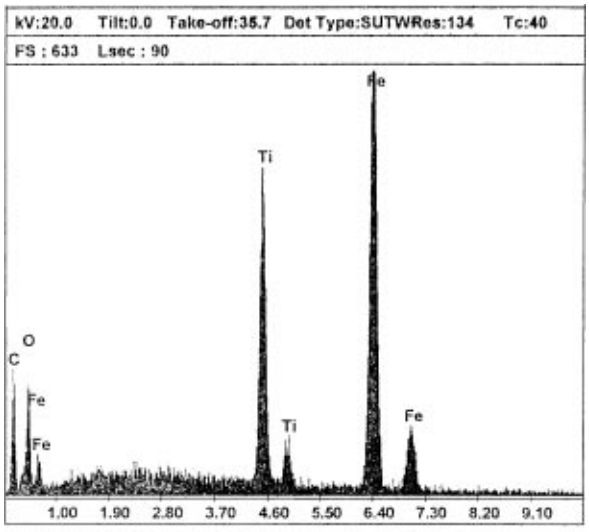

Element	Wt %	At %	K-Ratio	Z	A	F
C K	11.12	30.30	0.0283	1.1387	0.2231	1.0005
O K	10.87	22.24	0.0254	1.1193	0.2082	1.0017
TiK	17.75	12.13	0.1793	0.9559	0.9860	1.0715
FeK	60.26	35.33	0.5653	0.9548	0.9825	1.0000
Total	100.00	100.00				

(b)

Figure 8 (a) Typical SEM photomicrograph of wear scar on AISI 1045 steel rod, and (b) EDS analysis of (a), sliding against $Ti_{10\%}$-C : H or $Ti_{20\%}$-C : H coatings after wear testing for 5 min.

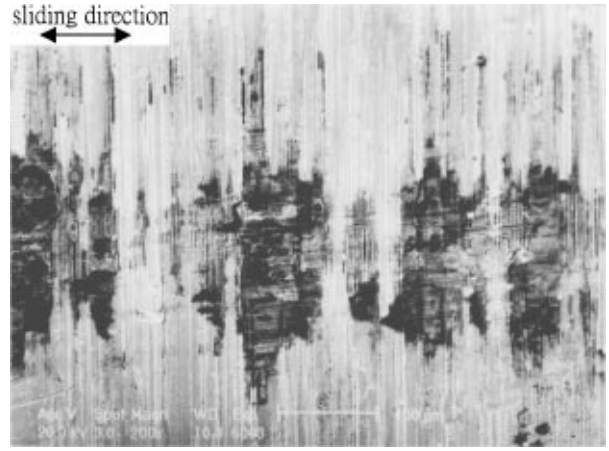

(a)

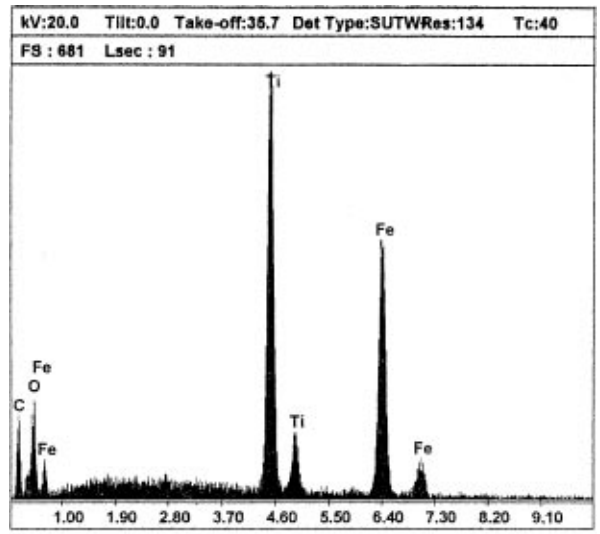

Element	Wt %	At %	K-Ratio	Z	A	F
C K	8.69	22.82	0.0242	1.1348	0.2447	1.0006
O K	15.99	31.51	0.0275	1.1155	0.1539	1.0009
TiK	33.72	22.19	0.3320	0.9521	0.9926	1.0419
FeK	41.60	23.48	0.3806	0.9506	0.9626	1.0000
Total	100.00	100.00				

(b)

Figure 9 (a) Typical SEM photomicrograph of wear scar on AISI 1045 steel rod, and (b) EDS analysis of (a), sliding against $Ti_{10\%}$-C : H or $Ti_{20\%}$-C : H coatings after wear testing for 10 min.

traces of friction coefficients are smooth and low in value. In addition, no wear debris and wear particles were observed in and out on the wear scar of the coated disk. Fig. 4a and b illustrate the typical tribological behavior (case 10, sliding against 1045 steel): the wear surface only had light rubbing traces and pits without any wear debris. Fig. 4b presents the EDS analysis corresponding to wear scar of Fig. 4a, which indicates that no Fe element transfer occurred from the counterbody 1045 steel rod. The similar wear and friction behavior occurred against the bronze rod that has a low coefficient of friction (see Table III). The typical wear surface as shown in Fig. 5 (case 10, sliding against bronze rod) displays only some mild rubbing traces but no wear debris on the wear scar of the coated disk. There was low wear depth on the coating film (see Table III) while the EDS analysis of Fig. 5 verified that no element adhesion to the coating film from the bronze rod was found. On the other hand, a transfer layer formed on the 1045 steel rod and the bronze rod. Fig. 6a and b display the typical wear scars of the 1045 steel rod and the bronze rod (sliding against case 11), respectively. In addition, original machining marks of the 1045 steel rod or the bronze rod can be clearly observed below the transfer layer. Friction behavior between the coated disk and this protective film on the 1045 steel rod or the bronze rod accounts for the positive effect on the tribological behavior because of a protective transfer layer formed on the 1045 steel rod or the bronze rod.

A different testing time analyzed the triboligical behavior between the contact surfaces of these wear pairs to discover why the coatings and the counterbodies (1045 steel rod and bronze rod) wore so mildly during the wear tests. Fig. 7a displays the typical wear scar of the 1045 steel (sliding against case 11) after testing 30 seconds. Some local contact surfaces of the 1045 steel rod had been plastic deformed which showed

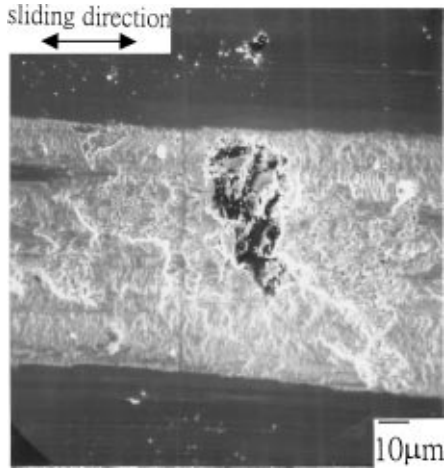

(a)

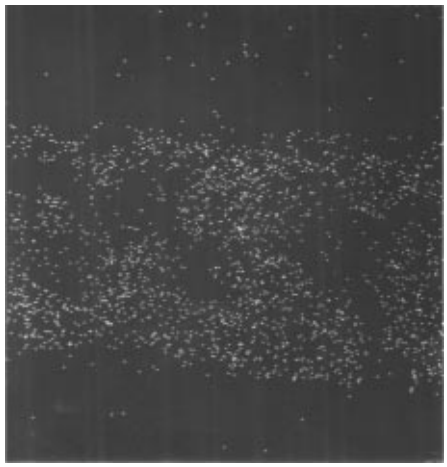

(b)

Figure 10 (a) Typical SEM photomicrograph of wear scar on the $Ti_{30\%}$-C : H coatings, and (b) WDS Fe map of (a), sliding against AISI 1045 steel after testing for 50 seconds.

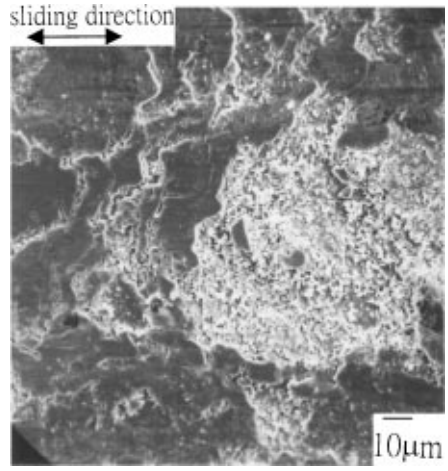

(a)

(b)

Figure 11 (a) Typical SEM photomicrograph of wear scar on AISI 1045 steel rod, and (b) WDS Ti map of (a), sliding against $Ti_{30\%}$-C : H coatings after wear testing for 50 seconds.

a smoother contact surface than the origin-machining surface. No element transfer occurred from coated disk to the wear scar on the 1045 steel rod as verified by EDS analysis of wear region of Fig. 7a as shown in Fig. 7b. The wear scar of 1045 steel rod formed a transferred layer as shown in Fig 8a after 5 minutes of testing. The EDS analysis of Fig. 8a verifies that the transferred layer is a rich-carbon transferred layer composed of a high amount of carbon as illustrated in Fig. 8b. The transferred layer regions were enlarged as displayed in Fig. 9a after 10 minutes of testing. The EDS analysis of the transferred layer regions displayed that the amount of carbon content decreased as the amount of Titanium and Oxygen increased as shown in Fig. 9b (compared with Fig. 8b). Finally, at the end of this experiment after 24 min the EDS analysis of Fig. 6a displayed that the transferred layer consists of 20.5% (atomic) carbon, 42% oxygen, 27.3% Ti, and 10.2% Fe. Therefore, its carbon content became stable at about 20% (atom) in the transferred layer. Obviously, a carbon-rich layer was formed on the counterbody 1045 steel rod which supplied a solid lubricant effected avoid the contact surfaces from a severe adhesion damage. The similar tribological behavior occurred to the coating/ bronze rod wear pairs

Group 2: The friction coefficient against the 1045 steel or the bronze shows a high value (as shown in Table III) when $x = 30\%$ in $Ti_{x\%}$-C : H coatings (case 7–9) or TiC/TiCN/TiN/Ti coating (case 12). This suggests that adhesive wear occurs under dry conditions. The wear test of short testing times was also performed to confirm that adhesion took place between the contact surfaces of these wear pairs. The maximum worn depth on a coated disk was only 1 μm (case 8, not worn out $Ti_{30\%}$-C : H coating with 2.5 μm) and the wear scar has ferric element adhesion from the counterbody 1045 steel rod, as verified by SEM photomicrographs and WDS Fe element mapping in Fig.10a and b, for the typical wear pair of $Ti_{30\%}$-C : H/1045 steel after 50 seconds of testing. Fig. 11a shows SEM photomicrograph of 1045 steel rod worn scar, and Fig. 11b shows the corresponding WDS Ti element mapping of Fig. 11a which reveals that the Ti element of the $Ti_{30\%}$-C : H coating film transferred to the 1045 steel rod worn scar. A typical wear scar of the coating (case 12: TiC/TiCN/TiN/Ti) sliding against the 1045 steel after testing 24 min. displayed in Fig. 12a displays a black compacted layer and some bright wear particles on the scar. The EDS analysis in Fig. 12b reveals that these compacted layers and particles are a mixture of oxides

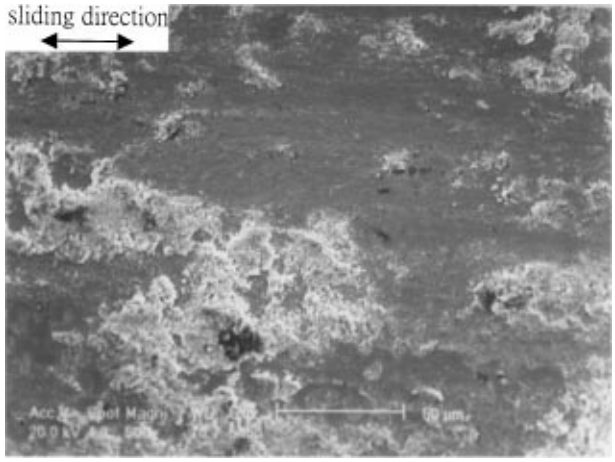

(a)

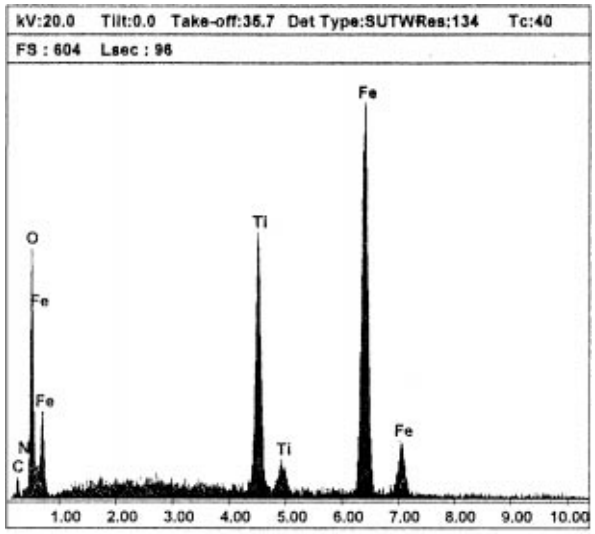

Element	Wt %	At %	K-Ratio	Z	A	F
C K	2.19	5.83	0.0056	1.1299	0.2242	1.0006
N K	1.23	2.80	0.0045	1.1198	0.3258	1.0018
O K	24.29	48.46	0.0651	1.1106	0.2409	1.0015
TiK	16.74	11.16	0.1673	0.9480	0.9873	1.0679
FeK	55.55	31.75	0.5176	0.9466	0.9844	1.0000
Total	100.00	100.00				

(b)

Figure 12 (a) Typical SEM photomicrograph of wear scar on TiC/TiCN/TiN/Ti coating, and (b) EDS analysis of (a), sliding against AISI 1045 steel rod after testing for 24 min.

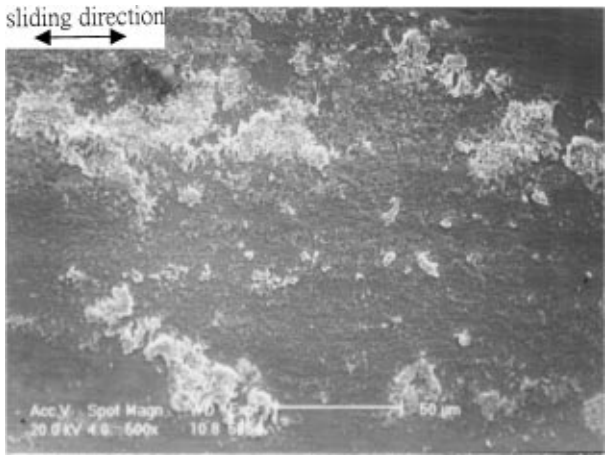

Figure 13 Typical SEM photomicrograph of wear scar on TiC/TiCN/TiN/Ti coating, sliding against bronze rod after testing for 24 min.

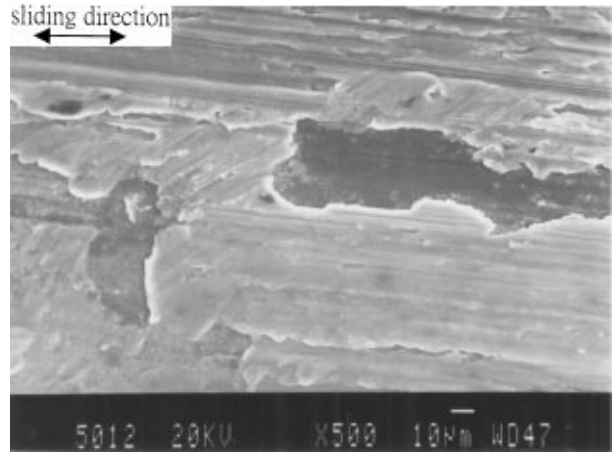

(a)

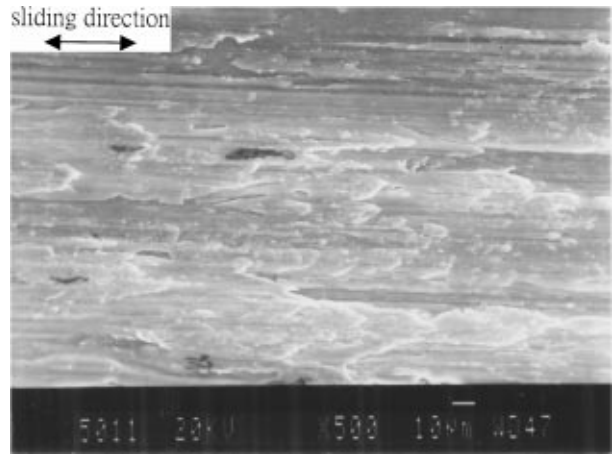

(b)

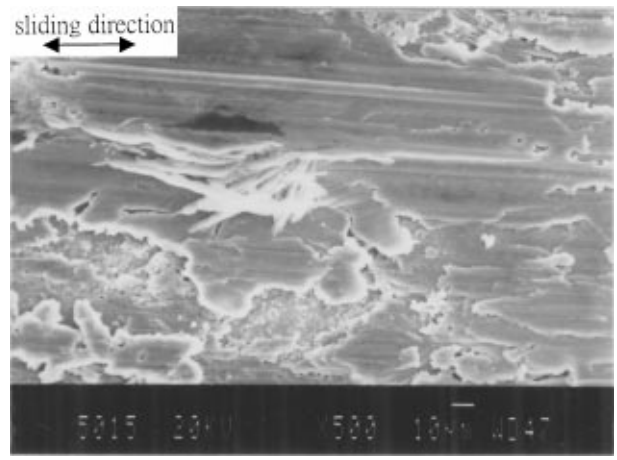

(c)

Figure 14 Typical SEM photomicrograph of Al transferred layer was formed on coating (case 3) for coating sliding against aluminum alloy (AA7075) after testing for (a) 3 seconds, for (b) 15 seconds, and for (c) 1 min.

from the two counterparts. The above analysis reveals that the 1045 steel/$Ti_{30\%}$-C : H coating or the 1045 steel/TiC/TiCN/TiN/Ti sliding pairs were damaged due to strong adhesive and tribo-oxidative wear. This damage is attributed to the fact that a low carbon content cannot supply an adequate amount of solid lubricant for the wear pairs. Similar wear and friction occurred for coatings (cases 7–9, and 12) against the bronze. Fig. 13a displays the typical wear scar of coating (case 12) sliding against the bronze. The EDS analysis

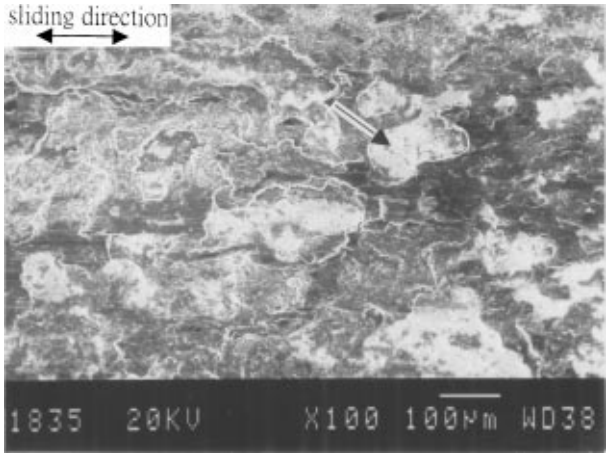

(a)

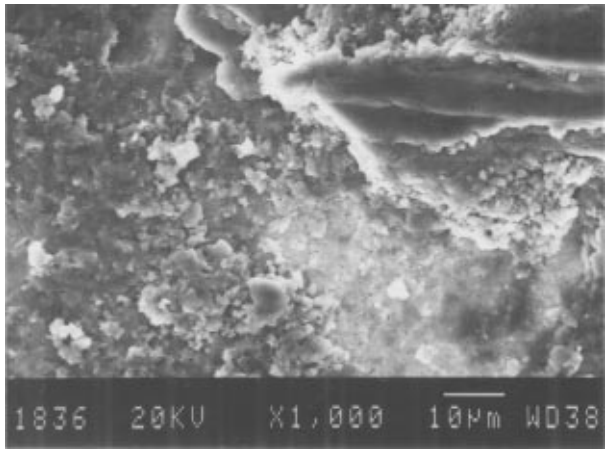

(b)

Figure 15 (a) Typical worn surface of coating (case 3), and (b) magnified of (a), for coating sliding against aluminum alloy (AA 7075) after testing 24 min.

of Fig. 13a reveals it consists of 8.4% (atomic) carbon, 4.4% nitrogen, 25.8% oxygen, 18.7% Ti, and 42.7% Cu.

4.2. $Ti_{x\%}$-C : H/7075 Al and $Ti_{x\%}$-C : H/6061 Al wear pairs

Fig. 14a, b, and c display the SEM photomicrographs of the transfer layer that formed on the coated disk (case 3) from the counterbody 7075 Al after 3 seconds, 15 seconds, and 1 min. of testing, respectively. The transfer layer formed on the $Ti_{x\%}$-C : H coating when wear tests were initially performed as shown in Fig. 14a. Then, the transferred layer was enlarged and covered the $Ti_{x\%}$-C : H coating as shown in Fig. 14b. Fig. 14c illustrated that some wear debris formed, delaminated, and spalled from the transferred layer, while Fig. 15a indicates that the worn surface of the coated disk (case 3: $Ti_{10\%}$-C : H coating with 3.5 μm thickness) after 24 min. test. The Al-transfer layer (black regions) that covered the worn coating and some local regions of transferred layer was delaminated, flaked, and the coating was pulled out. The WC substrate (bright regions, as indicated by an arrow) was then exposed. Fig. 15b, a magnification of Fig. 15a, demonstrates that the debris and small particles were composed of Al transferred layer mixed coating layer. An EDX analysis of the particles displayed that it consists of 34.39% (atomic) oxygen, 54.58% Al, 8.6% C and 2.43% Ti. Therefore, the Al transferred layer on the coating did not provide the protective effect for the coated disk, and severe damage on coating surface was thus produced by the adhesion process.

The wear mechanism for the 7075Al/coating or the 6061/coating sliding wear pairs can be summarized as follows: a transferred layer formed on the coating. The thickness of the transferred material over the coating increased during the wear process. The tribochemical reaction occurred on the contact surfaces and a mixed process of adhesion wear and oxidation wear occurred. Reciprocating sliding along with a high and large range fluctuation of the friction force through the wear test caused delamination and spallation of the transferred layer together with a catastrophic fracture in the coating.

5. Conclusion

$Ti_{x\%}$-C : H coatings with different contents of Titanium metal, coating thickness, and composition significantly differ in terms of tribological properties and wear mechanisms. The following conclusions are based on the results in this study:

1. The composition of $Ti_{x\%}$-C : H/TiC/TiCN/TiN/Ti with $x = 10\%$ and $x = 20\%$ level are the optimum coating designs for improvement of adhesion strength.

2. The optimum coating for wear resistance and friction against a 1045 steel or a bronze rod is $Ti_{10\%}$-C : H coating with 2.5 μm thickness. The $Ti_{x\%}$-C : H coatings with $x = 10\%$ and $x = 20\%$ have good tribology properties and also display very little counterbody wear. In contrast, even though it is harder, the $Ti_{x\%}$-C : H coatings at $x = 30\%$ or TiC/TiCN/TiN/Ti coating show a high friction coefficient and poor wear resistance.

3. Although the 6061 Al rod is not as hard as the 7075 Al rod, severe adhesion damage occurs for all the wear pairs of the 6061 Al or the 7075Al rod sliding against the coated disk. This damage results in delamination and spallation of the transfered layer together with a catastrophic fracture in the coating.

4. $Ti_{10\%}$-C : H or $Ti_{20\%}$-C : H coatings with good tribology characteristics can be employed as a coating pair with a carbon steel or copper alloy under dry conditions. However, it is less suitable to rub with aluminum alloy under dry conditions.

Acknowledgment

The authors would like to thank the National Science Council of the Republic of China for financially supporting this research under Contract No. NSC 87-2212-E006-046 and Cho Chang Tsung Foundation of Education for their financial support. Grateful thanks are specially dedicated to Mr. C. T. Wu for deposition.

References

1. H. TSAI and D. B. BOGY, *Jour. Vac. Sac. Tech.* **A5** (1987) 3287.
2. J. ROBERTSON, *Advan. Phys.* **35** (1986) 317.
3. A. ERDEMIR, M. SWITALA, R. WEI and P. WILBUR, *Surf. Coat. and Tech.* **50** (1991) 17.

4. D. KLAFKE, R. WASCHE and H. CZICHOS, *Wear* **153** (1992) 149.
5. Y. LIU, A. ERDENIR and E.I. MELETIS, *Surf. Coat. Tech.* **82** (1996) 48.
6. H. RONKAINEN, J. LIKOEN, J. KOSKINEN and S. VARJUS, *ibid.* **79** (1996) 87.
7. A. ERDEMIR, C. BINDAL, G. FENSKE and P. WILBUR, *Tribolog Transactions* **39** (1996) 735.
8. A. GRILL, B. S. MEYERSON and V. V. PATEL, *IBM J. Res. Develop.* **34**(6) (1990) 849.
9. G. ANDREW, KHURSHUDOV, MIKAEL OLSSON and KOJI KATO, *Wear* **205** (1997) 101.
10. D. P. MONAGHAN, D. G. TEER, P. A. LAING, I. EFEOGLU and R. D. ARNELL, *Surf. Coat. Technol.* **60** (1993) 525.
11. A. A. VOEVODIN, S. D. WALCK and J. S. ZABINSKI, *Wear* **203**/**204** (1997) 516.
12. M. D. BENTZON, K. MOGENSEN, J. B. HANSEN, C. TRAEHOLT, P. HOLIDAY and S. S. ESKILDSEN, *Surf. Coat. Techol.* **68**/**69** (1994) 651.
13. J. KOSKINEN, H. RONKAINEN, J. P. HIRVONEN, R. LAPPALAINEN and K. A. PISCHOW, *Diamond Relat. Mater.* **4** (1995) 843.
14. S. ANDERS, A. ANDERS, J.W. AGER III, Z. WANG, G. M. PHARR, T. Y. TSUI, I. G. BROWN and C. S. BHATIA, *Mater. Res. Soc. Symp. Proc.* **383** (1995) 453.
15. S. J. HARRIS, A. M. WEINER and W. J. MENG, *Wear* **211** (1997) 208.
16. J. DENG and M. BRANU, *Diamond and Related Materials* **4** (1995) 936.
17. M. WANG, K. SCHMIDT and K. REICHELT, *J. Mater. Res.* 7(**3**) (1992) 667.
18. R. M. GERMAN, "Powder Metallurgy Science" (Metal Power Industries Federation, Princeton, 1994) p. 241.
19. Y. SATO, M. KAMO and N. SETAKA, *Carbon* **16** (1978) 279.
20. A. IMAMURA, ET AL., *Surf. Coat. Tech.* **36** (1988) 161.
21. V. KULIKOVSKY, ET AL., *Diamond and Related Materials* **7** (1998) 774.

Received 9 July 1999
and accepted 8 June 2000